Letters

Adaptive Extremum Seeking Control Based *LCL* Filter Resonant Frequency Online Estimation

Yuheng Wu, *Student Member, IEEE*, Mohammad Hazzaz Mahmud, *Student Member, IEEE*, Radha Sree Krishna Moorthy, *Member, IEEE*, Madhu Chinthavali, *Senior Member, IEEE*, and Yue Zhao, *Senior Member, IEEE*

***Abstract*—The *LCL* filter has been widely used in the grid-tied inverter systems. However, the resonance of the *LCL* filter can reduce the system stability margin and the control performance. Moreover, the grid impedance variations can lead to the drift of the resonant frequency, which can further worsen the system robustness. Thus, it is important to know the actual resonant frequency of the *LCL* filter. In this letter, an adaptive extremum seeking control (AESC) based estimation scheme is proposed to estimate the resonant frequency of the *LCL* filter online. By injecting a high-frequency (HF) signal into the inverter output voltage, the AESC scheme can identify the extremum of the *LCL* filter amplitude response, i.e., resonant peak. The amplitude of injection signal is adaptive based on the inverter HF response, which can address the tradeoff between the dynamic response and inverter output current quality. Most importantly, compare to other method, the proposed scheme has very low computational complexity, which minimizes the burden to the normal inverter controller operation. Stability analysis is given in this letter, and experimental studies are conducted to validate the effectiveness of the proposed scheme.**

***Index Terms*—Adaptive extremum seeking control (AESC), low computational complexity, resonant frequency estimation.**

I. Introduction

COMPARED with the *L*-type filter, the *LCL* filter can provide better switching ripple attenuation with reduced filter volume, and thus, the *LCL* filter has been widely used in grid-tied inverter systems. However, the resonance of the *LCL* filter deteriorates the stability of the inverter system [1]. Moreover, the grid impedance variation can lead to the drift of the resonant frequency, which can turn the notch-filter-based active damping schemes ineffective and worsen the system robustness and stability [1], [2]. Thus, it is important to know the resonant frequency of the *LCL* filter online, which can benefit the design of adaptive active damping schemes and provide the information of grid-side impedance [1]–[5].

In [1], the resonance of the *LCL* filter is excited by tuning the controller first, and then the estimation of the resonant frequency can be achieved by using discrete Fourier transform (DFT). Based on the estimated resonant frequency, the notch-filter-based active damping scheme can be adaptive [1] and the grid impedance can also be calculated [3]. In [6], the parameters of the *LCL* filter are estimated by a recursive prediction error (RPE) algorithm, whereas a binary sequence is injected into the inverter output voltage to excite the resonance of the filter. The recursive least square (RLS) scheme is combined with the RPE scheme to estimate the parameters of the *LCL* filter in [7], whereas the pseudorandom binary sequence is used as the excitation signal. However, both DFT scheme and recursive algorithms suffer from the heavy computation burden, which may even affect the normal operation of the inverter controller.

In this letter, an adaptive extremum seeking control (AESC) based estimation scheme is proposed to estimate the resonant frequency of the *LCL* filter in real time. The extremum seeking control (ESC) algorithm can find the setpoint that extremizes the system output without known plant dynamics [8]. By injecting a high-frequency (HF) signal into the inverter output voltage, the AESC scheme can seek the frequency that can maximize the excited response, which is the resonant frequency of the *LCL* filter. Compared with the conventional ESC scheme, where a constant amplitude signal is injected, the proposed AESC scheme can actively adjust the amplitude of the injection signal, which can address the tradeoff between the scheme dynamic response and the inverter output current quality. The stability analysis of the AESC scheme is given, and experimental studies have been conducted to validate the effectiveness of the proposed scheme. Compared with the DFT scheme and recursive estimation schemes, the AESC scheme has much lower computational complexity, which can benefit the real-time realization and allow the implementation on low-cost microcontrollers.

Manuscript received May 17, 2021; revised June 15, 2021 and July 17, 2021; accepted July 26, 2021. Date of publication August 4, 2021; date of current version September 16, 2021. This work was supported by the Oak Ridge National Laboratory funded through the Department of Energy—Office of Electricity's, Transformer Resilience and Advanced Components program led by the program manager Andre Pereira. (*Corresponding author: Yue Zhao*.)

Yuheng Wu, Mohammad Hazzaz Mahmud, and Yue Zhao are with the Power Electronic Systems Laboratory at Arkansas, University of Arkansas, Fayetteville, AR 72701 USA (e-mail: yuhengwu@uark.edu; mhmahmud@uark.edu; yuezhao@uark.edu).

Radha Sree Krishna Moorthy and Madhu Chinthavali are with the Electrical Energy Systems Integration Group, Oak Ridge National Laboratory, Knoxville, TN 37932 USA (e-mail: krishnamoorr@ornl.gov; chinthavalim@ornl.gov).

Color versions of one or more figures in this article are available at https://doi.org/10.1109/TPEL.2021.3102063.

Digital Object Identifier 10.1109/TPEL.2021.3102063

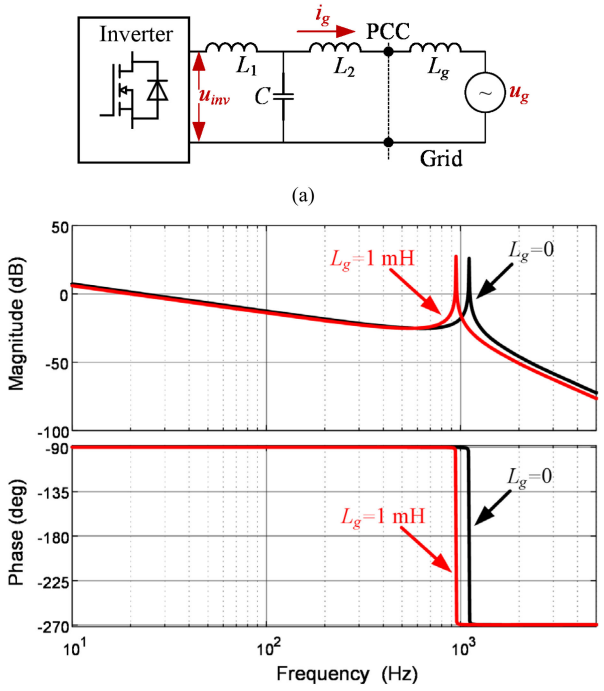

Fig. 1. (a) Grid-tied inverter with an *LCL* filter and (b) typical frequency response of the *LCL* filter.

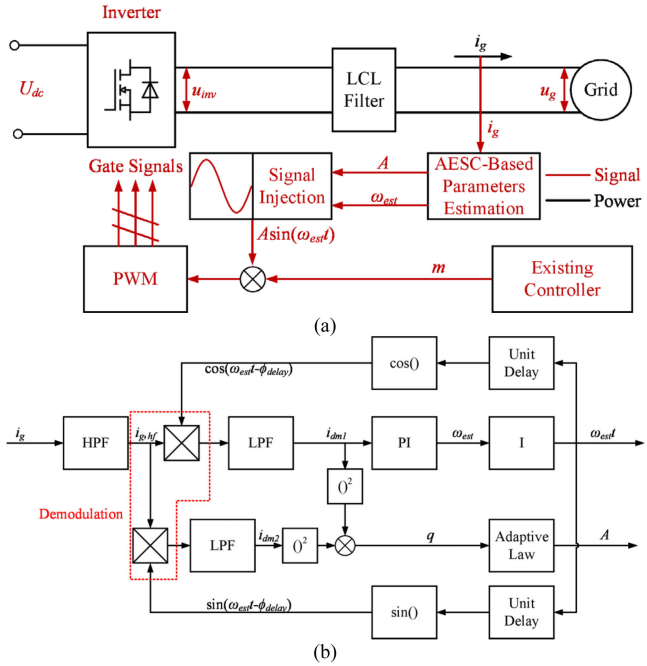

Fig. 2. AESC-based resonant frequency estimation scheme: (a) inverter-level system diagram and (b) detailed diagram of AESC.

II. AESC-Based *LCL* Filter Resonant Frequency Estimation

A. AESC-Based Estimation Scheme

Fig. 1(a) shows the schematic of the *LCL*-type grid-tied inverter, where the *LCL* filter consists of L_1, C, and L_2, L_g is the grid impedance, u_{inv} is the output voltage of the inverter, u_g represents the grid voltage, i_g is the grid-side current, and PCC is the point of common coupling. In this work, the grid impedance is considered as inductive. Besides, the number of resonances is supposed as one, i.e., there is only one resonant frequency in the grid-tied inverter system. The grid-side current i_g satisfies

$$i_g(s) = \frac{u_{\text{inv}}(s) - \left(1 + L_1 C s^2\right) u_g(s)}{s\left[L_1\left(L_2 + L_g\right) C s^2 + L_1 + L_2 + L_g\right]} \tag{1}$$

and the resonant frequency is $\omega_r = \sqrt{\frac{L_1+L_2+L_g}{L_1(L_2+L_g)C}}$. As an example, Fig. 1(b) shows the frequency response of the *LCL* filter under different grid impedances. It can be seen that the grid impedance can notably impact the resonant frequency of the *LCL* filter.

Fig. 2(a) shows the inverter-level system diagram, where the AESC-based estimation scheme is integrated with an existing controller, i_g is grid-side current, A is the amplitude of the injection signal, ω_{est} is the estimated resonant frequency of the *LCL* filter, and m is the output of the existing controller. The AESC scheme samples grid-side current i_g and provides the estimation of the resonant frequency ω_{est} as well as the amplitude of the injection signal A. Then, the signal injection block injects a HF signal $A\sin(\omega_{\text{est}}t)$ into the inverter output voltage to excite the *LCL* filter. Fig. 2(b) shows the detailed diagram of the proposed scheme, where HPF is the high-pass filter, $i_{g,\text{hf}}$ is the HF response of the grid-side current excited by the injection signal, LPF is the low-pass filter, i_{dm1} and i_{dm2} are the outputs of the low-pass filters, respectively, q is the input of the adaptive law, PI is the proportional-integral controller, I is the integrator, and the unit delay blocks are used to cancel the one-step delay caused by the digital control.

With the signal injection, the grid-side current can be written as

$$i_g(t) = I_{\text{fund}} \sin\left(\omega_{\text{fund}} t + \phi_{\text{fund}}\right) + B \sin\left(\omega_{\text{est}} t + \phi_1 - \phi_{\text{delay}}\right) \tag{2}$$

where ω_{fund} is the grid fundamental frequency, ϕ_{fund} is the phase angle of the fundamental current, I_{fund} is the amplitude of the fundamental grid-side current, B is the amplitude of the HF response of the grid-side current that is excited by the injection signal, ϕ_1 is the phase angle of the *LCL* filter at frequency ω_{est}, and ϕ_{delay} is the phase delay caused by the digital control. Assuming the HPF can eliminate the fundamental component, and the extracted HF response of i_g can be written as

$$i_{g,\text{hf}}(t) = C \sin\left(\omega_{\text{est}} + \phi_1 + \phi_2 - \phi_{\text{delay}}\right) \tag{3}$$

where C is the amplitude of the extracted signal and ϕ_2 is the phase angle of the HPF at frequency ω_{est}. It should be noted that a properly design HPF should provide high attenuation performance at the fundamental frequency and introduce low amplitude and phase angle distortions at frequency ω_{est}, i.e., $C \approx B$ and $\phi_2 \approx 0$. Besides the signal injection, the estimated resonant frequency is also used to demodulate the HF grid-side current. In the cosine demodulation branch, the demodulated

signal is

$$\cos\left(\omega_{\text{est}}t-\phi_{\text{delay}}\right)\times i_{\text{g,hf}}=\frac{C}{2}\times\left[\underbrace{\sin\left(\phi_1+\phi_2\right)}_{\text{constant}}\right.$$
$$\left.+\underbrace{\sin\left(2\omega_{\text{est}}+\phi_1+\phi_2-2\phi_{\text{delay}}\right)}_{\text{double-frequency}}\right]. \tag{4}$$

Similarly, the demodulated signal in the sine branch is

$$\sin\left(\omega_{\text{est}}t-\phi_{\text{delay}}\right)\times i_{g,\text{hf}}=\frac{C}{2}\times\left[\underbrace{\cos\left(\phi_1+\phi_2\right)}_{\text{constant}}\right.$$
$$\left.-\underbrace{cos\left(2\omega_{\text{est}}+\phi_1+\phi_2-2\phi_{\text{delay}}\right)}_{\text{double-frequency}}\right]. \tag{5}$$

It can be seen that both demodulated signals consist of low-frequency components and double-frequency components. Especially, the low-frequency components, i.e., $\cos(\phi_1+\phi_2)$ and $\sin(\phi_1+\phi_2)$, contain the phase angle of the *LCL* filter. Thus, the LPFs are used to remove the double-frequency components and extract the low-frequency components. Supposing a properly designed LPF can totally remove the double-frequency components, the outputs of the low-pass filters can be written as

$$\begin{cases} i_{dm1}=\frac{C}{2}\sin\left(\phi_1+\phi_2\right) \\ i_{dm2}=\frac{C}{2}\cos\left(\phi_1+\phi_2\right). \end{cases} \tag{6}$$

As mentioned earlier, a properly designed HPF should satisfy $\phi_2\approx 0$. Based on the frequency response of the *LCL* filter given in Fig. 1(b), signal i_{dm1} satisfies

$$\begin{cases} i_{dm1}<0, \omega_{\text{est}}<\omega_r \\ i_{dm1}=0, \omega_{\text{est}}=\omega_r \\ i_{dm1}>0, \omega_{\text{est}}>\omega_r. \end{cases} \tag{7}$$

Thus, a PI controller is used to seek the estimated frequency that can lead to $i_{dm1}=0$, where the estimated frequency is the same as the resonant frequency of the *LCL* filter.

It should be noticed that under a constant amplitude of injection signal, i.e., *A* is a constant, the amplitudes of HF response, i.e., *B* and *C*, vary at different ω_{est}. In other words, the amplitude response of the *LCL* filter, which is given in Fig. 1(b), determines the ratio *B*/*A*. It can be seen that at the resonant frequency, the ratio *B*/*A* is much larger than that at different frequencies. Small amplitude of injection signal is preferred to improve the inverter output power quality with slow dynamic response. In contrast, a large amplitude *A* can improve the dynamic response of the proposed scheme at the cost of steady-state current quality. To address the tradeoff between the power quality of inverter and the dynamic response of the proposed scheme, an adaptive law is adopted to actively adjust the amplitude of the injection signal. Based on Fig. 2(b) and (6), the input of the adaptive law satisfies

$$q=i_{dm1}^2+i_{dm2}^2=\frac{C^2}{4} \tag{8}$$

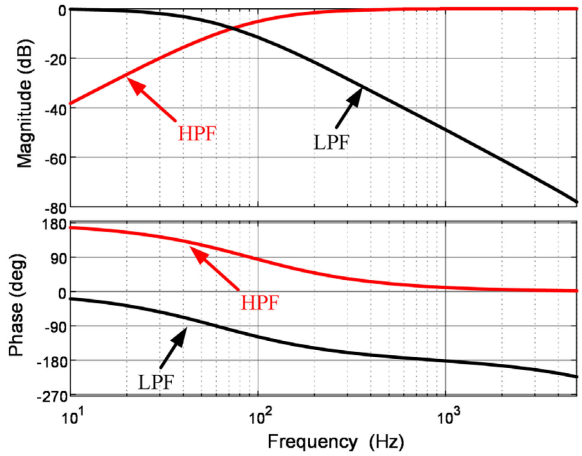

Fig. 3. Frequency response of the designed HPF and LPF.

which means q can represent the amplitude of the HF response of i_g. Thus, a simple adaptive law is adopted as

$$A=\frac{J}{2\sqrt{q}+\lambda} \tag{9}$$

where $J>0$ is a constant that limits the maximum amplitude of the injection signal, and $\lambda>0$ is a constant that can avoid dividing zero. With the adaptive law (9), the AESC scheme can decrease the amplitude of the injection signal when ω_{est} approaches ω_r, and thus, the inverter output current quality can be improved. Meanwhile, a large amplitude of the injection signal will be used when ω_{est} is far from the resonant frequency, which can enhance the dynamic response of the proposed scheme.

Remark 1: With the estimated resonant frequency of the *LCL* filter, i.e., ω_{est}, it is possible to calculate the grid impedance. According to Liserre *et al*. [3], assuming *LCL* filter parameters are known, and the grid impedance is inductive, i.e., the grid impedance can be represented by L_g shown in Fig. 1(a). The resonant frequency of the *LCL* filter without grid impedance can be calculated as $\omega_{r,\text{LCL}}=\sqrt{\frac{L_1+L_2}{L_1L_2C}}$.In the steady state, define $\Delta=\omega_{\text{est}}^2-\omega_{r,\text{LCL}}^2$to represent the difference of resonant frequency caused by the grid impedance. Then, the grid impedance can be calculated as $L_g=L_2(\frac{1}{1+L_2C\Delta}-1)$.

B. AESC Design and Stability Analysis

As mentioned earlier, the HPF eliminates the fundamental component from the grid-side current, whereas the LPFs remove the double-frequency components from the demodulated signals. Here, a second-order HPF is used to reduce the complexity. Its transfer function can be written as

$$\text{HPF}\left(s\right)=\frac{s^2}{\left(s+\alpha\right)^2} \tag{10}$$

where α is the bandwidth of the HPF. It can be seen from (6) that the accuracy of the estimation scheme depends on the phase angle of the HPF at the estimated frequency, i.e., ϕ_2. Meanwhile, the bandwidth of the HPF also determines the attenuation of the fundamental grid-side current. In this work, the bandwidth

of the HPF is set as 1.5 times of the fundamental frequency, i.e., $\alpha = 1.5\omega_{\rm fund}$, which can provide about 10-dB attenuation performance.

The LPFs need to remove the double-frequency components from the demodulated signals. However, as the LPFs and the PI controller are inside of the feedback loop, the stability of the proposed scheme should be analyzed. Supposing second-order LPFs are adopted, which can be written as

$$\mathrm{LPF}\,(s) = \frac{\beta^2}{(s+\beta)^2} \tag{11}$$

where β is the bandwidth of the LPF. The PI controller can be written as

$$\mathrm{PI}\,(s) = k_p + \frac{k_i}{s} \tag{12}$$

where k_p and k_i are the gains of the PI controller. To simplify the controller design, the ratio between k_i and k_p is set as β, i.e., $k_{\rm i} = \beta k_p$. Based on Fig. 2(b), the estimated resonant frequency satisfies

$$\frac{d\omega_{\rm est}}{dt} = k_p \frac{di_{dm1}}{dt} + k_i i_{dm1}. \tag{13}$$

Define the estimation error e as $e = \omega_r - \omega_{\rm est}$, and a Lyapunov function V can be defined as

$$V = \frac{1}{2}e^2. \tag{14}$$

Supposing the actual resonant frequency ω_r is slow time-varying. The derivative of V can be calculated as

$$\frac{dV}{dt} = e\frac{de}{dt} = -e\frac{d\omega_{\rm est}}{dt} = -e\left(k_p \frac{di_{dm1}}{dt} + k_i i_{dm1}\right). \tag{15}$$

Define an intermediate variable p that satisfies

$$p = \frac{1}{\beta}\left(\frac{di_{dm1}}{dt} + \beta i_{dm1}\right). \tag{16}$$

Actually, the intermediate variable p can be regarded as the output of a virtual first-order LPF $\beta/(s+\beta)$, and the input of the virtual LPF is the same as that of the LPF shown in Fig. 2(b). With the variable p, (15) can be rewritten as

$$\frac{dV}{dt} = -e\left(k_p \frac{di_{dm1}}{dt} + k_i i_{dm1}\right) = -e\beta k_p p. \tag{17}$$

The intermediate variable p also satisfies (7) by replacing i_{dm1} with p if the virtual LPF can effectively attenuate the double-frequency components. Thus, based on the Lyapunov criterion, the proposed scheme is stable if $k_p<0$.

According to the aforementioned stability analysis, it can be seen that the design of the LPF filter bandwidth should be low enough to reject the double-frequency component. In practice, the resonant frequency ω_r usually is much high than the fundamental frequency $\omega_{\rm fund}$. In this article, the bandwidth β is set the same as the fundamental frequency, i.e., $\beta = \omega_{\rm fund}$. Fig. 3 shows the frequency responses of the designed HPF and LPF.

Remark 2: Compared with the recursive estimation schemes [6], [7], [12], the complicated matrix computation is avoided in the proposed scheme. Based on Fig. 2(b), Table I summarized the operation and the complexity of the proposed scheme, where the complexity is presented by using the big O notation [12].

TABLE I
SUMMARY OF THE PROPOSED SCHEME

Operation	Complexity
$N^{\rm th}$-order HPF	$O(N)$
Demodulation	$O(1)$
$N^{\rm th}$-order LPF	$O(N)$
Square Operation: $()^2$	$O(1)$
PI and I	$O(1)$
Adaptive Law	$O(1)$
Unit Delay	$O(1)$
cos() and sin()	$O(1)$

It can be seen from Table I that except for the LPF and HPF, the complexity of all the other blocks shown in Fig. 2(b) is in the order of $O(1)$. Considering the order of the LPF and HPF is N, the overall computational complexity of the proposed scheme is in the order of $O(N)$. The complexity of the RLS scheme is $O(N^2)$ [12], where N is the number of parameters to be estimated. Thus, the proposed scheme has much lower complexity compared with the recursive estimation schemes. As an example, in this work, the order of filters is set as $N = 2$, whereas the number of parameters to be estimated in [6] and [7] is $N = 5$.

III. Experimental Studies

To validate the effectiveness of the proposed scheme, experimental studies have been conducted. Fig. 4 shows the experiment setup, where a grid simulator is used to simulate the grid, a single-phase inverter with *LCL* filter is used as the grid-tied inverter, and the controller is implemented on a dSPACE MicroLabBox. The resonant frequency of the *LCL* filter is $\omega_r =$ 1200 Hz. The parameters of the AESC scheme are set as $\alpha =$ 90 Hz, $\beta = 60$ Hz, $J = 0.5$, $\lambda = 0.1$, and $k_p = 100$.

Fig. 5 shows the experiment results. The initial value of the estimated resonant frequency $\omega_{\rm est,init}$ is set higher and lower than ω_r in Fig. 5(a) and (b), respectively, to validate the convergence performance from both directions. The proposed scheme can achieve convergence within three fundamental cycles in both tests. Moreover, the adaptive law can actively adjust the amplitude of the injection signal to tradeoff between dynamic response and steady-state current quality. Fig. 6 shows the estimation performance under a highly distorted grid. Similar to the results given in Fig. 5, the proposed scheme can provide satisfactory estimation result even under highly distorted grid voltage and current. Besides, Fig. 7 shows the estimation performance of the proposed scheme under the weak grid condition, where an additional 1-mH inductor is added between PCC and grid simulator to represent the grid impedance L_g. Due to the grid impedance, the resonant frequency of the *LCL* filter reduces to 900 Hz, and the proposed scheme can still provide an accurate estimation of the actual resonant frequency.

To compare the computational complexity of the proposed scheme with recursive estimation schemes presented in [6] and [7], the proposed scheme and RLS scheme have been implemented in both the MicroLabBox and a TI DSP TMS320F28335.

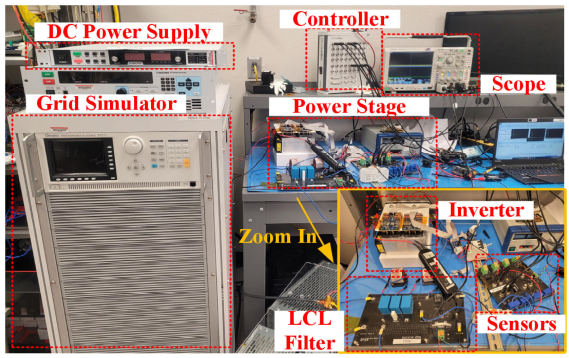

Fig. 4. Experiment setup.

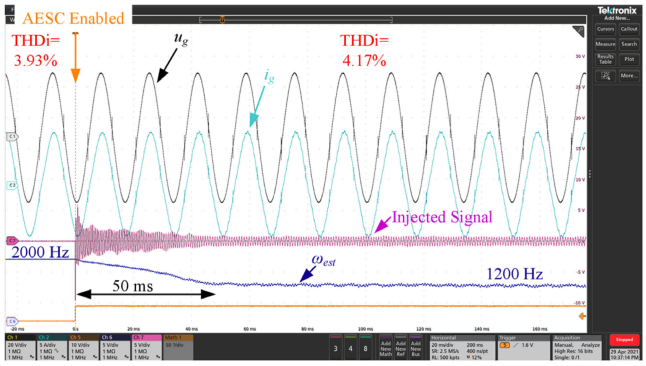

(a)

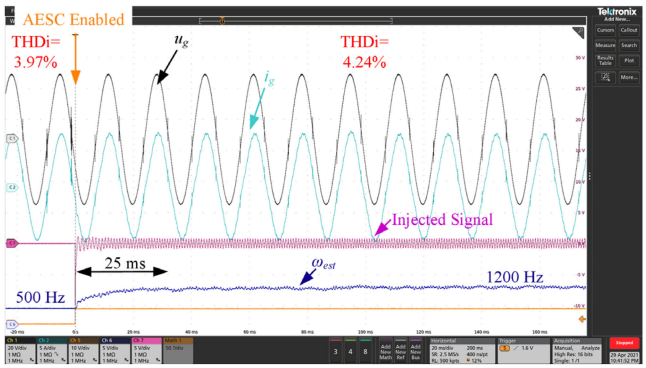

(b)

Fig. 5. Performance of proposed scheme with differential initial conditions: (a) $\omega_r < \omega_{\mathrm{est,init}}$ and (b) $\omega_r > \omega_{\mathrm{est,init}}$.

The code for MicroLabBox is generated and downloaded into MicroLabBox by using Simulink Coder. The code for the TI DSP is also generated by MATLAB/Simulink and downloaded to the DSP by using Code Composer Studio. The measurement of the execution time follows the guides that are provided by dSPACE and MATLAB, respectively [10], [11]. In the MicroLabBox, the execution time of the proposed scheme is 1.1 μs, whereas the RLS scheme needs 2.2 μs. Similarly, the proposed scheme costs 18.5 μs in the TI DSP, whereas the RLS scheme costs 68.3 μs, which means that the proposed scheme has much less computational complexity and is more suitable for real-time applications.

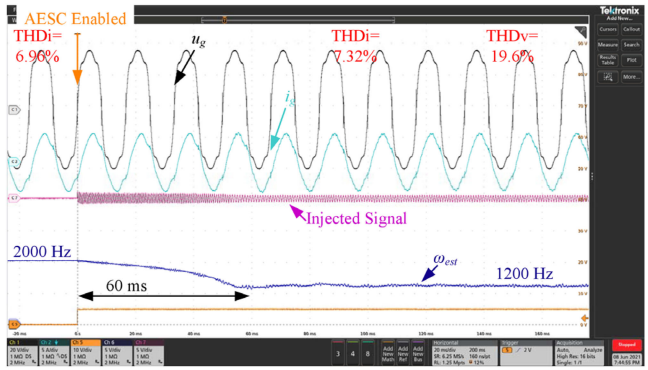

Fig. 6. Performance of proposed scheme under highly distorted grid.

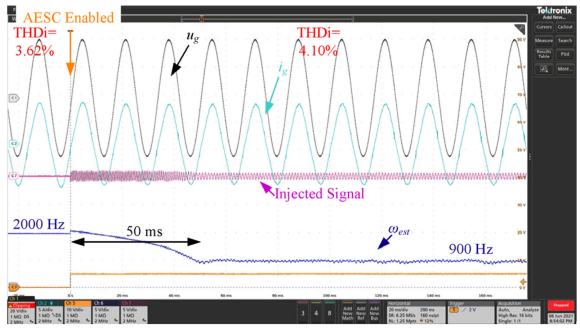

(a)

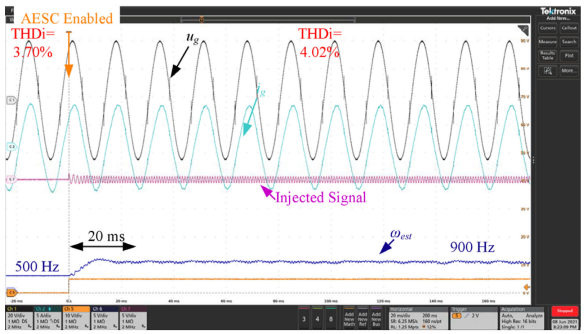

(b)

Fig. 7. Performance of proposed scheme under weak grid with differential initial conditions: (a) $\omega_r < \omega_{\mathrm{est,init}}$ and (b) $\omega_r > \omega_{\mathrm{est,init}}$.

IV. Conclusion

An AESC-based *LCL* resonant frequency estimation scheme is proposed in this letter. By injecting a HF signal into the inverter output voltage, the AESC scheme can seek the actual resonant frequency of the *LCL* filter in real time. Besides, the adaptive law of the AESC scheme can actively adjust the amplitude of injection signal to address the tradeoff between dynamic performance and steady-state current quality. The proposed scheme has much less computational complexity compared with the state-of-the-art solutions. Stability analysis is presented to guide the controller design, and experimental studies have been conducted to demonstrate the effectiveness of the proposed scheme.

REFERENCES

[1] R. Peña-Alzola, M. Liserre, F. Blaabjerg, M. Ordonez, and T. Kerekes, "A self-commissioning notch filter for active damping in a three-phase *LCL*-filter-based grid-tie converter," *IEEE Trans. Power Electron.*, vol. 29, no. 12, pp. 6754–6761, Dec. 2014.

[2] W. Wu, Y. Liu, Y. He, H. S. Chung, M. Liserre, and F. Blaabjerg, "Damping methods for resonances caused by *LCL*-filter-based current-controlled grid-tied power inverters: An overview," *IEEE Trans. Ind. Electron.*, vol. 64, no. 9, pp. 7402–7413, Sep. 2017.

[3] M. Liserre, F. Blaabjerg, and R. Teodorescu, "Grid impedance estimation via excitation of *LCL*-filter resonance," *IEEE Trans. Ind. Appl.*, vol. 43, no. 5, pp. 1401–1407, Sep./Oct. 2007.

[4] A. V. Timbus, R. Teodorescu, F. Blaabjerg, and U. Borup, "Online grid measurement and ENS detection for PV inverter running on highly inductive grid," *IEEE Trans. Power Electron.*, vol. 2, no. 3, pp. 77–82, Sep. 2004.

[5] P. García, M. Sumner, Á. Navarro-Rodríguez, J. M. Guerrero, and J. García, "Observer-based pulsed signal injection for grid impedance estimation in three-phase systems," *IEEE Trans. Ind. Electron.*, vol. 65, no. 10, pp. 7888–7899, Oct. 2018.

[6] V. Pirsto, J. Kukkola, F. M. M. Rahman, and M. Hinkkanen, "Real-time identification of *LCL* filters employed with grid converters," *IEEE Trans. Ind. Appl.*, vol. 56, no. 5, pp. 5158–5169, Sep./Oct. 2020.

[7] J. Koppinen, J. Kukkola, and M. Hinkkanen, "Plug-in identification method for an *LCL* filter of a grid converter," *IEEE Trans. Ind. Electron.*, vol. 65, no. 8, pp. 6270–6280, Aug. 2018.

[8] K. B. Ariyur and M. Krstić, *Real Time Optimization by Extremum Seeking Control*. New York, NY, USA: Wiley, 2003.

[9] *Embedded Coder Support Package for Texas Instruments C2000 Processor*. 2021, [Online]. Available: https://www.mathworks.com/help/supportpkg/texasinstrumentsc2000/index.html?s_tid=CRUX_lftnav

[10] *Real-Time Code Execution Profiling*. 2021, [Online]. Available: https://www.mathworks.com/help/supportpkg/texasinstrumentsc2000/ug/real-time-code-execution-profiling.html

[11] *Measuring Execution Times of Blocks and Subsystems*. 2019, [Online]. Available: https://www.dspace.com/shared/support/faqpdf/faq023.pdf

[12] J. Jiang and Y. Zhang, "A revisit to block and recursive least squares for parameter estimation," *Comput. Elect. Eng.,* vol. 30, no. 5, pp. 403–416, Jul. 2004.